

# Thermal conduction in molecular materials using coarse grain dynamics: Role of mass diffusion and quantum corrections for molecular dynamics simulations

Ya Zhou and Alejandro Strachan<sup>a)</sup>*School of Materials Engineering, Purdue University, West Lafayette, Indiana 47907, USA*

(Received 29 April 2009; accepted 17 November 2009; published online 21 December 2009)

We use a mesodynamical method, denoted dynamics with implicit degrees of freedom (DID), to characterize thermal transport in a model molecular crystal below and above its melting temperature. DID represents groups of atoms (molecules in this case) using mesoparticles and the thermal role of the intramolecular degrees of freedom (DoFs) are described implicitly using their specific heat. We focus on the role of these intramolecular DoFs on thermal transport. We find that thermal conductivity is independent of intramolecular specific heat for solid samples and a linear relationship between the two quantities in liquid samples with the coefficient of proportionality being the mass diffusivity of the mesoparticles. As the temperature of the liquids is increased, thermal conductivity exhibits an increased sensitivity with respect to the specific heat of the internal DoFs due to the enhanced molecular mobility. Based on these results, we propose a simple method to incorporate quantum corrections to thermal conductivity obtained from nonequilibrium molecular dynamics simulations of molecular liquids. Our results also provide insight into the development of thermally accurate coarse grain models of soft materials. © 2009 American Institute of Physics. [doi:10.1063/1.3272028]

## I. INTRODUCTION

Thermal processes and management of molecular materials at small size scales are essential in a wide range of fields from active cooling of computer chips to bioengineering. Fluids with dispersed nanoscale-size particles (nanofluids) often exhibit anomalously high thermal conductivity and are being considered as materials for next-generation coolants.<sup>1,2</sup> Biological systems, on the other hand, contain proteins and other biomolecules that interact with water and must maintain a certain function temperature.<sup>3–5</sup> Many therapeutic practices, e.g., cancer hyperthermia, also involve controlling heat transfer in body tissues by exposing them to high temperatures.<sup>6,7</sup> Despite significant recent advances, such as the characterization of thermal transport in molecular chains using ultrafast heat bursts<sup>8</sup> and the effect of base fluid viscosity on thermal conductivity of nanofluids,<sup>9</sup> progress in these areas is hindered by the lack of fundamental understanding of the molecular mechanisms of heat transfer in complex, nanostructured molecular materials, and the lack of predictive and computationally efficient simulation tools. Experimental efforts remain challenging due, in part, to the small temporal and spatial scales involved and the very restricted capabilities of measuring thermal conduction at the nanoscale.<sup>10</sup> While atomic-level simulations have the potential to provide a quantitative and qualitative understanding, several challenges remain to be solved.

Classical, all-atom molecular dynamics (MD) is a very powerful technique to understand atomic scale phenomena with an unparalleled level of detail. However, such atomistic

simulations are computationally intensive and remain restricted to relatively small systems and short time scales (linear dimensions of tens to hundreds of nanometers and nanosecond timescales using today's supercomputers). Also, being based on classical mechanics (rather than quantum), MD leads to an inaccurate description for materials below their Debye temperatures (where the fundamental energy of some vibrational modes  $h\nu$  is larger than the thermal energy  $kT$ ). For molecular materials at room temperature, the overestimation of the specific heat given by a classical description can be so significant that the thermal properties of the materials are falsely described. Coarse grain or mesodynamical simulations, where groups of atoms are described by mesoparticles, provide a computationally less intensive alternative to all-atom MD and, consequently, the possibility to simulate more realistic timescales and structures. These techniques are widely used in simulations of soft materials including polymers,<sup>11,12</sup> molecular crystals, and biomaterials<sup>13,14</sup> and are computationally less expensive than MD because of two reasons: (i) a reduction in the number of degrees of freedom (DoFs) and (ii) longer time steps of integration since high frequency vibrational modes are not explicitly described. The mechanical effects of the intermolecular DoFs are described via an interparticle interaction potential (or mesopotential) that *averages* the atomic interactions. However, the intramolecular DoFs also play a thermal role, i.e., they exchange energy with the explicit DoFs, which is often neglected or treated very crudely in coarse grain simulations. Recently, a mesodynamical method was proposed, which incorporates the thermal role of intramolecular DoFs in mesoscale simulations and leads to a thermodynamically accurate description.<sup>15</sup> This approach, de-

<sup>a)</sup>Electronic mail: strachan@purdue.edu.

noted dynamics with implicit DoFs (DID), uses local, finite thermostats to describe the thermal role of the DoFs internal to each mesoparticle.<sup>15</sup> Furthermore DID enables the incorporation of quantum thermal effects that limit the accuracy of all-atom MD.

In this paper, we use DID to characterize thermal transport in a model molecular material. We focus on the role of the specific heat associated with localized DoFs internal to the mesoparticles for solid and liquid samples. The remainder of the paper is organized as follows: In Sec. II, we describe the DID model and simulation details. In Secs. III and IV, we present our results and discuss the different role of internal specific heat in thermal transport in solid and liquid samples. In Sec. V, we discuss the implication of our results to make quantum corrections to all-atom MD simulations of thermal transport in molecular fluids. Finally, in Sec. VI, conclusions are drawn.

## II. MODEL AND SIMULATION DETAILS

### A. DID

The simulations are carried out using the DID equations of motion<sup>15</sup> that describe the temporal evolution of the positions and velocities of mesoparticles and that of an additional internal variable per mesoparticle, the internal temperature, which describes their internal state

$$\begin{aligned}\dot{\mathbf{r}}_i &= \mathbf{u}_i + \nu \left( \frac{T_i^{\text{meso}} - T_i^{\text{int}}}{\theta^0} \right) \frac{\mathbf{F}_i}{m_i \langle \omega^2 \rangle}, \\ \dot{\mathbf{u}}_i &= \frac{\mathbf{F}_i}{m_i}, \\ \dot{T}_i^{\text{int}} &= \nu \left( \frac{T_i^{\text{meso}} - T_i^{\text{int}}}{\theta^0} \right) \frac{|\mathbf{F}_i|^2}{C_i^{\text{int}} m_i \langle \omega^2 \rangle},\end{aligned}\quad (1)$$

where  $\mathbf{r}_i$  is the position,  $\mathbf{u}_i$  the velocity,  $m_i$  the mass, and  $\mathbf{F}_i$  is the force acting on mesoparticle  $i$ .  $T_i^{\text{meso}}$  and  $T_i^{\text{int}}$  are the local mesoparticle (molecular) and internal temperatures of mesoparticle  $i$ ,  $\theta^0$  is a reference temperature (equilibrium temperature of the system in our simulations), and  $\langle \omega^2 \rangle$  is the mean square frequency of the interparticle vibrational modes. The thermal energy of the internal DoFs of mesoparticle  $i$  is described by the internal specific heat  $C_i^{\text{int}}$  (in our case all the mesoparticles are identical and they have the same specific heat). According to Eq. (1), energy exchange between mesoparticles and their internal DoFs occurs when there is a difference between the local mesoparticle temperature around particle  $i$  ( $T_i^{\text{meso}}$ ) and the temperature of its internal DoFs ( $T_i^{\text{int}}$ ). This energy exchange leaves the total energy of the system unchanged,

$$E^{\text{tot}} = E^{\text{meso}} + E^{\text{int}}, \quad (2)$$

where  $E^{\text{meso}}$  is the sum of the potential and kinetic energies of all the mesoparticles

$$E^{\text{meso}} = V(\{\mathbf{r}_i\}) + \sum_i \frac{1}{2} m_i \mathbf{u}_i^2, \quad (3)$$

and  $E^{\text{int}}$  is a function of the internal temperature of each mesoparticle

$$E^{\text{int}} = \sum_i E_i^{\text{int}}(T_i^{\text{int}}). \quad (4)$$

The description of the thermal properties of the internal DoFs can be understood as a finite, local thermostat associated with each mesoparticle, which takes energy away from the mesoparticle when  $T_i^{\text{meso}} > T_i^{\text{int}}$  and gives energy to the mesoparticle when  $T_i^{\text{meso}} < T_i^{\text{int}}$ . The rate of energy exchange is determined by the coupling rate  $\nu$ .

It should be noted that the model based on Eq. (1) is the simplest possible version of DID where the internal state of the mesoparticles can be described with an energy-temperature relationship leading to a constant specific heat. These equations are trivially generalized for temperature-dependent specific heat necessary to capture effects of quantum statistical mechanics. An additional assumption in Eq. (1) is that the internal state of the mesoparticles can be described by a single parameter, the internal temperature  $T^{\text{int}}$ . However, in some applications, structural transformations of intramolecular DoFs take place as a result of large temperature and/or pressure change, and the coarse graining process involved in DID would lead to an inaccurate description of the thermodynamic state due to reduced DoFs.<sup>16</sup> For such problems, the DID method should be extended to allow more general relationships between  $E^{\text{int}}$  and  $T^{\text{int}}$  that may depend on additional internal variables. In addition, besides the features of the method itself, the capability of DID to truthfully describe the behavior of a material strongly relies on the capability of the mesopotentials to describe the interaction between mesoparticles under the thermodynamic conditions of interest. As described in Sec. II B, these mesopotentials can be obtained from first principle calculations or experiments.

### B. Model molecular material

The goal of this study is to understand the role of intramolecular DoFs on thermal transport in molecular materials using DID. Consequently, we consider a generic molecular material that crystallizes in the fcc structure. The mesoparticles interact with each other via a simple many-body, embedded atom model potential that was parametrized to describe thermal and mechanical properties of Al systems;<sup>17</sup> this allows us to compare current results to our previous work on Al using regular MD.<sup>18</sup> The results of this paper are insensitive to the choice of interaction potential between the mesoparticles (mesopotential). For simulations of specific materials an appropriate mesopotential should be used that correctly captures the effective interactions between particles. These potentials can be parametrized using all-atom MD simulations<sup>15,19</sup> or from experimental data. Mesogained or coarse-grained potentials are available for a wide range of materials including metals,<sup>20</sup> polymers,<sup>12</sup> molecular crystals,<sup>21</sup> etc.

Within the DID description [Eq. (1)], two parameters are used to describe the thermal properties of the implicit DoFs of a material: (i) the coupling rate  $\nu$  which determines the rate of energy exchange between the mesoscopic and internal DoFs, and (ii) the internal specific heat  $C^{\text{int}}$  which relates the thermal energy of the internal DoFs and their temperature.

The coupling rate  $\nu$  determines the strength of the coupling between the intermolecular and intramolecular DoFs. This parameter depends on how the intramolecular DoFs couple with the mesoscale ones and the anharmonicities of the rotovibrational density of states of the material. In realistic systems, the value of coupling rate can be obtained from all-atom MD calculations<sup>15</sup> or from experimental data. In this paper we vary this coupling rate from 0 to 20.66 ps<sup>-1</sup> to explore its role on thermal transport. This range contains the value we used previously for a DID representation of a crystalline polymer.<sup>15</sup>

The specific heat of molecular materials exhibits strong temperature dependence due to quantum thermal effects and DID can be used with a temperature-dependent  $C^{\text{int}}$ . This can be done with a simple modification to Eq. (1). However, in this paper, we take the internal specific heat to be independent of temperature, which is a good approximation to the behavior one would obtain in classical all-atom MD simulations with harmonic internal DoFs. In this case, the internal specific heat is related to the number of atomic DoFs per mesoparticle

$$C^{\text{int}} = N^{\text{int}}k_B = (3N^{\text{atom}} - 3)k_B, \quad (5)$$

where  $k_B$  is Boltzmann's constant,  $N^{\text{int}}$  is the number of internal DoFs of each mesoparticle, and  $N^{\text{atom}}$  is the number of atoms contained in each mesoparticle. For DID simulations of specific materials, an accurate expression for the internal specific heat should be used. This can be obtained from first principles using quantum statistical mechanics and the rotovibrational density of states from MD, molecular statistics or experiments; for example, specific heat of water can be calculated using classical MD with quantum corrections.<sup>22</sup>

In order to illustrate how DID brings internal and explicit DoFs to equilibrium we simulate an fcc molecular system consisting of 500 mesoparticles. The system is constructed by replicating a four-molecule fcc unit cell five times in each direction. Figure 1(a) shows the temporal evolution of the molecular and internal temperatures for mesoparticles with  $C^{\text{int}}$  of  $1k_B$  and  $10k_B$  and  $\nu$  of 2.066 ps<sup>-1</sup>, which is an intermediate value in the range of coupling rate we explore in this work, at constant energy. We start from a perfect crystal and assign velocities corresponding to an initial instantaneous temperature of 300 K. Since the initial positions of the mesoparticles correspond to the ground state of the system (lowest possible potential energy) and remembering that classical mechanics predicts that in equilibrium the total energy will be divided approximately equally between kinetic and potential energies (principle of equipartition of energy), we expect that about half of the initial kinetic energy of the mesoparticles will be transformed into potential energy within a short period of time (of the order of a molecular vibration). This process leaves the mesoparticles with a temperature of about 150 K while their internal tempera-

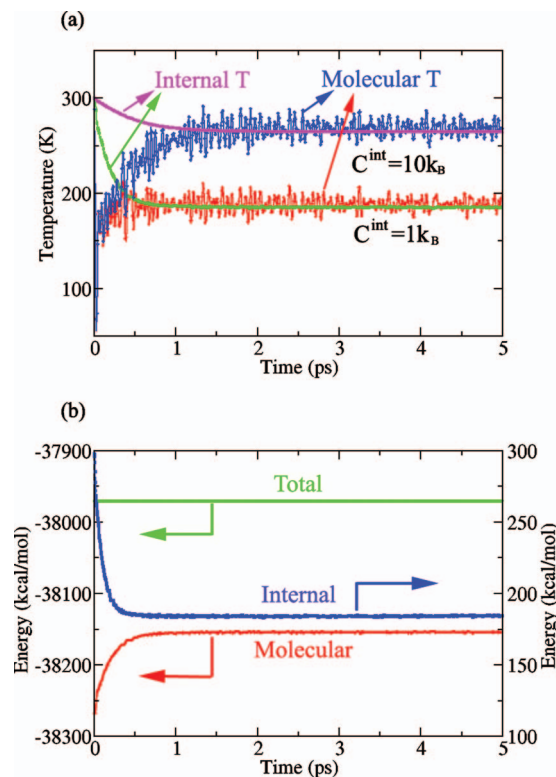


FIG. 1. Temporal evolution of (a) temperatures and (b) energies in a mesoparticle system at 300 K with a coupling rate of 2.066 ps<sup>-1</sup>. Curves in (a) correspond to internal specific heats of  $1k_B$  and  $10k_B$ , respectively. Molecular and internal temperatures equilibrate quickly in both cases. A larger internal specific heat leads to an equilibrium temperature closer to 300 K. With an internal specific heat of  $1k_B$ , the molecular and internal energies in (b) equilibrate at the same rate as that of temperature equilibration in (a); the total energy of the system is conserved.

ture will remain closer to the initial value of 300 K (transferring energy between the internal DoFs and the mesoparticles requires several molecular vibrations). At this point, the internal DoFs, working as local thermostats, begin to transfer energy to the mesoparticles, leading to a decrease in the internal temperature and an increase in the mesoparticle temperature. This process continues until the temperatures associated with both sets of DoFs converge to the same value. This process of equilibration can be seen in Fig. 1(a) for the same structure of two different values of internal specific heat. Increasing  $C^{\text{int}}$  from  $1k_B$  to  $10k_B$  increases the amount of thermal energy stored in the intramolecular DoFs and, therefore, leads to an equilibrium temperature closer to 300 K, the initial temperature of the internal DoFs. Note that in the limit of infinite  $C^{\text{int}}$  and if all mesoparticles are assigned identical initial internal temperatures the DID method reduces to Berendsen thermostat.<sup>23</sup> As indicated by the mesodynamics equations of motion [Eq. (1)], while the molecular and internal temperatures equilibrate, the energy exchange between the mesoscopic and internal DoFs leaves the total energy of the system unchanged. This can be seen in Fig. 1(b), where we show the temporal evolution of the total, meso, and internal energies during the DID simulation corresponding to  $C^{\text{int}}=1k_B$ . As energy is transferred from intramolecular to intermolecular DoFs, the molecular energy increases and the internal energy decreases. As expected

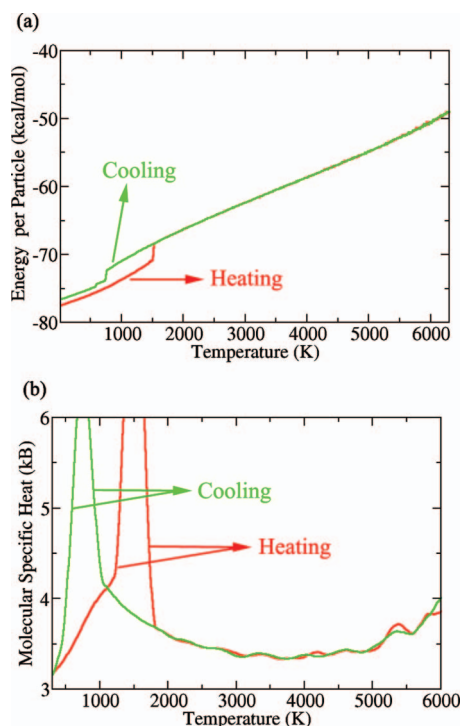


FIG. 2. (a) External energy (sum of potential and kinetic energy) per mesoparticle with temperature. (b) Molecular specific heat calculated from the curves in (a). Running average of the data is taken to average out numerical errors and obtain  $C^{\text{mol}}$  for further calculation.

from the DID equations the total energy of the system is conserved, which provides an important verification to our DID implementation.

### C. Molecular specific heat

The total specific heat of the material is obtained as a sum of the contribution of the implicit DoFs ( $C^{\text{int}}$ ) and that of the mesoparticle DoFs, or molecular specific heat ( $C^{\text{mol}}$ ),

$$C^{\text{tot}} = C^{\text{mol}} + C^{\text{int}}. \quad (6)$$

We calculate  $C^{\text{mol}}$  for our model material from external mesoparticle energy versus temperature curves obtained from MD simulations of the abovementioned  $5 \times 5 \times 5$  fcc molecular system. We heat the system up from  $T = 10$  K to 6300 K with a temperature increment of 10 K; at each temperature we perform a 25-ps-long MD simulation under constant pressure and temperature conditions ( $NPT$  ensemble) with zero pressure, and use the last 20 ps of each run to compute the averages. We cool the system down in the same manner. Figure 2(a) shows the total mesoparticle energy (potential plus kinetic energies,  $E^{\text{meso}}$  in DID) as a function of temperature. The isobaric specific heat as a function of temperature can be calculated from the data as the derivative of enthalpy with respect to temperature. Since the pressure is zero in the simulations we consider the  $P(\partial V / \partial T)$  term to be negligible and write the molecular specific heat as the derivative of energy with respect to temperature

$$C^{\text{mol}}(T) = \left. \frac{\partial E^{\text{meso}}(T)}{\partial T} \right|_P. \quad (7)$$

We compute the derivative numerically by fitting the energy versus temperature data to straight lines in a series of overlapping temperature range of  $T \pm 200$  K. The data show scatter that is typical in numerical derivatives of atomistic quantities, and therefore we take a running average over a 200 K period from  $T - 100$  K to  $T + 100$  K to smooth the curve. Figure 2(b) shows  $C^{\text{mol}}$  as a function of temperature calculated from the heating and cooling curves in Fig. 2(a). In the heating curve, a sharp peak is observed at  $\sim 1500$  K due to the latent heat associated with melting. For this temperature range,  $C^{\text{mol}}$  is obtained from the cooling curve to avoid possible overestimation.  $C^{\text{mol}}$  at other temperatures in our discussion below are obtained from the heating curve.

### D. Thermal conductivity calculation and simulation details

In this study, thermal conductivity is calculated using a nonequilibrium MD (NEMD) method proposed by Müller-Plathe.<sup>24</sup> In general, NEMD methods are known to be able to provide reasonably accurate lattice thermal conductivity for nonmetals<sup>25</sup> as well as metallic systems.<sup>18,26</sup> In the current approach, a known heat flux is imposed on the system and the associated steady-state temperature gradient that develops is measured. The heat flux and the temperature gradient are collinear and the thermal conductivity is obtained via Fourier's law<sup>24</sup>

$$\kappa = - \frac{J}{dT/dz}, \quad (8)$$

where  $J$  is the heat flux and  $dT/dz$  is the temperature gradient in steady state.

The molecular system under study is an fcc crystal consisting of 4000 mesoparticles (with initial structure obtained by replicating the four-atom fcc unit cell  $5 \times 5 \times 40$  times along the three  $\langle 100 \rangle$  crystallographic directions) with periodic boundary conditions in all three directions. The system is evenly divided into 40 slabs along the  $[001]$  direction and the slabs are labeled as slabs 1 to 40 from left to right. Slab 1 is defined as the cold slab and slab 21 the hot one. Heat flux is imposed in the longitudinal direction by swapping the velocity vectors of the mesoparticle with the highest kinetic energy in the cold slab and the one with the lowest kinetic energy in the hot slab. During this process, the internal temperatures and energies of the two mesoparticles remain unchanged. A time step of 1 fs is used to integrate the equations of motion and the velocities are swapped every 192 time steps. The total simulation time is 1920 ps, which corresponds to a total of 10 000 velocity swaps. As heat is transferred from the cold to the hot slabs by velocity swapping, the molecular temperature is directly affected and the internal temperature responds accordingly in presence of a non-zero coupling rate  $\nu$ . The mesoscopic and internal DoFs remain in or near equilibrium as a temperature gradient develops between the hot and cold slabs. Once steady state is achieved the average heat flux and the temperature gradient

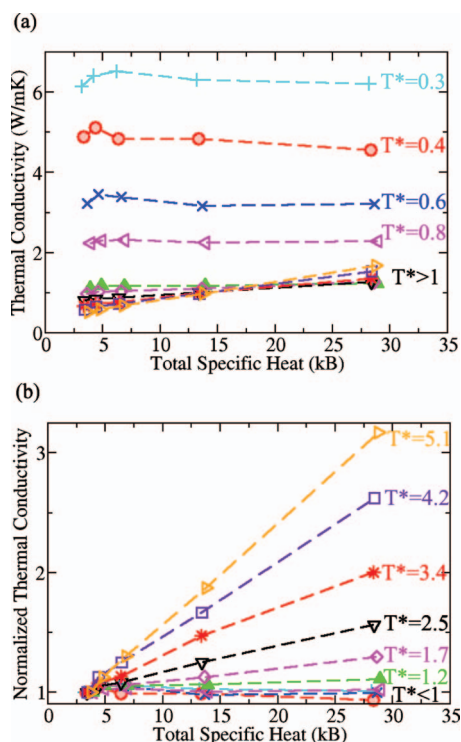


FIG. 3. Thermal conductivity as a function of specific heat over a wide range of temperature. Data corresponding to each nominal temperature  $T^*$  are shown with the same symbol in (a) and (b). (a) Thermal conductivity shows dependence on specific heat only in liquid samples. (b) Normalized thermal conductivity vs. specific heat. The thermal conductivities for each temperature are normalized by the value corresponding to zero  $C^{\text{int}}$ . Thermal conductivity remains very constant as specific heat changes at  $T^* < 1$ , while a strong linear correlation is observed at elevated temperatures.

are used to compute thermal conductivity. We explore the role of internal DoFs in thermal transport by varying  $\nu$  between 0 and  $20.66 \text{ ps}^{-1}$  and  $C^{\text{int}}$  in the range of  $0k_B$ – $25k_B$ . For the coupling rates used, the temperature profiles become stationary typically after several hundred picoseconds. Consequently, the thermal conductivities associated with intramolecular and intermolecular temperatures are calculated based on Eq. (8), using heat flux and temperature gradient averaged over the second half of the simulation time (from 960–1920 ps). The two values of thermal conductivity are very similar because the molecular and internal temperatures are in equilibrium during this time period. Thermal conductivity of the mesoparticle system is then considered as the average of the two.

### III. SIMULATION RESULTS

We first focus on the effect of internal specific heat on thermal conductivity over a wide temperature range. To generalize our results for the model molecular material system, we scale the temperatures by the equilibrium melting temperature  $T_m$  corresponding to the potential used, and define a dimensionless nominal temperature  $T^* = T/T_m$ .  $T_m$  is estimated to be 1180 K from the heating and cooling curves in Fig. 2(a) (an  $\sim 20\%$  overestimation compared to the experimental value for Al).<sup>27</sup> Figure 3(a) shows thermal conductivity as a function of total specific heat ( $C^{\text{tot}}$ ) at a series of nominal temperatures from 0.3 to 5.1. Note that simulations

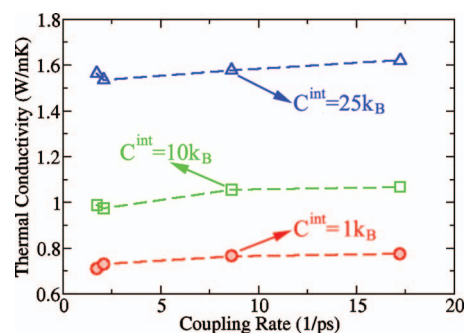


FIG. 4. Thermal conductivity with coupling rate at  $T^* = 4.2$  with  $C^{\text{int}}$  of  $3k_B$  (circles),  $10k_B$  (squares), and  $25k_B$  (triangles). The effect of coupling constant is very weak compared with that of  $C^{\text{int}}$ .

for  $C^{\text{int}} = 0k_B$  correspond to regular MD and are performed by reducing the coupling constant  $\nu$  to zero. Since  $C^{\text{mol}}$  has a constant value for each temperature, the dependence of thermal conductivity on  $C^{\text{tot}}$  at a given temperature is the result of change in  $C^{\text{int}}$ . For  $C^{\text{int}} = 0k_B$  (leftmost data point for each temperature), thermal conductivity decreases with increasing temperature due to enhanced phonon scattering. More interestingly, thermal conductivity is rather insensitive to  $C^{\text{int}}$  for  $T^*$  up to 0.8 but increases noticeably at higher temperatures. The dependency of thermal conductivity on  $C^{\text{int}}$  is more evident in Fig. 2(b), where thermal conductivity at each temperature is normalized by the value corresponding to  $C^{\text{int}} = 0k_B$ . While thermal conductivity at  $T^* = 0.3$  remains almost constant, there is a small increase in thermal conductivity at  $T^* = 1.2$  as  $C^{\text{int}}$  increases from  $0k_B$  to  $25k_B$ . At  $T^* = 2.5$  a linear correlation between thermal conductivity and  $C^{\text{int}}$  is readily observed and the correlation becomes even stronger as temperature further increases. We note that the dependence of thermal conductivity on  $C^{\text{int}}$  becomes observable at temperatures above  $T_m$ ; this effect will be discussed in detail in Sec. IV.

The thermal properties of the intramolecular DoFs are determined not only by  $C^{\text{int}}$ , but also the coupling rate  $\nu$  that describes their coupling with the molecular DoFs. We now investigate the role of  $\nu$  on thermal conduction and, since thermal conductivity of the solid samples is insensitive with respect to  $C^{\text{int}}$ , we focus on systems at temperatures above  $T_m$ . Figure 4 shows thermal conductivity as coupling rate changes at  $T^* = 4.2$  for three different values of  $C^{\text{int}}$ . The effect of coupling rate on thermal conduction is very weak compared with that of  $C^{\text{int}}$ . While increasing  $C^{\text{int}}$  from  $3k_B$  to  $25k_B$  more than doubles the thermal conductivity, increasing the coupling rate almost tenfold leads to scatter of the data within 10%.

### IV. DISCUSSION

The DID results presented in Sec. III can be summarized as follows: thermal conductivity of molecular solids is insensitive to the specific heat of localized intramolecular DoFs; in liquid samples with significantly higher molecular mobility a linear relationship between thermal conductivity and internal specific heat is observed. In this section we discuss the meaning and implications of these results.

The behavior of solid samples can be understood from the solid-state physics point of view. Thermal conductivity of a system can be obtained by solving the Boltzmann transport equation. Within the Debye approximation, the phonon thermal conductivity is simplified as<sup>28</sup>

$$\kappa = \frac{1}{3} \int_0^{\theta_D k_B / \hbar} C(\omega) v l(\omega) d\omega, \quad (9)$$

where  $\omega$  is the vibrational frequency of phonons,  $\theta_D$  is the Debye temperature,  $C$  is the heat capacity at constant volume,  $v = d\omega/dk$  is the group velocity of phonons, and  $l$  is the phonon mean free path.

In crystalline materials with multiple atoms in the unit cell, the phonon dispersion curves consist of both acoustic and optical branches. The high frequency optical branches corresponding to intramolecular modes show very little dispersion in molecular materials since they involve strong covalent bonds, whereas intermolecular DoFs are associated with much weaker van der Waals and electrostatic interactions. Therefore the optical phonons associated with intramolecular modes have small group velocities and conduct heat very inefficiently. The intramolecular DoFs described implicitly in DID represent dispersionless optical modes with zero group velocity, and according to Eq. (9), they should not contribute to thermal conduction. Our numerical simulations confirm this behavior and provide an important validation for the DID equations of motion.

In amorphous and liquid materials with no structural periodicity, the concepts of  $k$ -space and phonon dispersion become meaningless and both Eq. (9) and our arguments to explain the independence of thermal conductivity and internal specific heat are not applicable. Furthermore, in liquid samples we observe a linear relationship between thermal conductivity and internal (or total) specific heat; we would like to understand this behavior and predict the value of the proportionality coefficient between these two properties. Thermal conductivity of liquid and amorphous systems can be expressed as an integral over each vibrational mode with frequency  $\omega$  (Ref. 29)

$$\kappa = \int C(\omega) D(\omega) n(\omega) d\omega, \quad (10)$$

where  $D(\omega)$  is the energy diffusion coefficient and  $n(\omega)$  represents the density of states. The frequency-independent counterpart of  $D(\omega)$  is the thermal diffusivity  $\alpha$ , which is the ratio of thermal conductivity to volumetric heat capacity

$$\alpha = \frac{\kappa}{\int C(\omega) n(\omega) d\omega} = \frac{\kappa}{C_v}, \quad (11)$$

where  $C_v = C^{\text{tot}}/V_{\text{mol}}$  is the specific heat per unit volume (with unit of J/m<sup>3</sup> K) with  $V_{\text{mol}}$  being the volume of the mesoparticle. From the shape of the curves in Figs. 3(a) and 3(b), we see that  $\alpha$  for our molecular material depends both on temperature and  $C_v$  (via the internal specific heat  $C^{\text{int}}$ ).

For molecular materials, Eq. (10) can be rewritten to separate the contributions of the intermesoparticle and intramesoparticle DoFs as

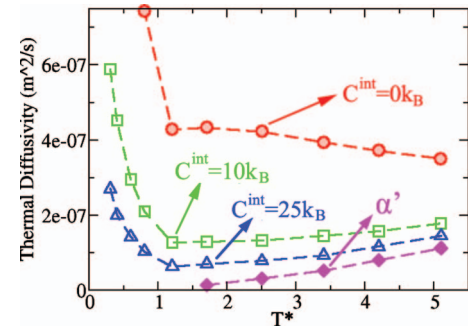


FIG. 5. Thermal diffusivity and local thermal diffusivity with nominal temperature  $T^*$ . Thermal diffusivity generally decreases with temperature in the low temperature regime. At a given temperature, thermal diffusivity decreases with increasing  $C^{\text{int}}$ . The local thermal diffusivity  $\alpha'$  increases with temperature in liquid samples.

$$\kappa = \frac{1}{V_{\text{mol}}} \sum_{\omega}^{\text{inter}} C^{\text{mol}}(\omega) D^{\text{mol}}(\omega) + \frac{C^{\text{int}}}{V_{\text{mol}}} \sum_{\omega}^{\text{intra}} D^{\text{int}}(\omega), \quad (12)$$

where  $D^{\text{mol}}$  and  $D^{\text{int}}$  are the energy diffusion coefficients of the explicit and internal DoFs, respectively. Based on our DID results for liquid samples we also define a “local” thermal diffusivity  $\alpha'$ , which better captures the observed linear correlation between thermal conductivity and  $C^{\text{int}}$ ,

$$\alpha' = V_{\text{mol}} \frac{\partial \kappa}{\partial C^{\text{int}}}. \quad (13)$$

Due to the linear correlation between thermal conductivity and  $C_v$ , we obtain  $\alpha'$  as the slope of the data shown in Fig. 3. While thermal diffusivity  $\alpha$  depends both on temperature and  $C^{\text{int}}$ , our simulations show that the local thermal diffusivity  $\alpha'$  is independent of  $C^{\text{int}}$  (i.e., it is independent of the internal DoFs). The temperature dependence of the local thermal diffusivity and thermal diffusivity corresponding to  $C^{\text{int}} = 0k_B$ ,  $10k_B$ , and  $25k_B$  is shown in Fig. 5. As expected, thermal diffusivity decreases in solids up to the melting temperature. The trends for liquid samples depend on the value of  $C^{\text{int}}$ . Thermal diffusivity of  $C^{\text{int}} = 0k_B$  liquids decreases with temperature, while in the two other cases ( $C^{\text{int}} = 10k_B$  and  $25k_B$ ) thermal diffusivity increases with temperature. The local thermal diffusivity also increases with increasing temperature in liquid samples.

The temperature dependence of the local thermal diffusivity  $\alpha'$  and Eq. (12) point to a possible connection between  $\alpha'$  and mass diffusivity. We calculate the mass diffusion coefficient  $D_{\text{mass}}$  as a function of temperature from mesoparticle mean square displacement as a function of time<sup>30</sup> obtained from DID simulations. The diffusion coefficient for materials with various values of  $C^{\text{int}}$  is shown in Fig. 6 as a function of temperature. The internal DoFs (described by  $C^{\text{int}}$ ) have a negligible effect on mass diffusion, providing an additional evidence that the DID’s approach to couple molecular and internal DoFs does not introduce nonphysical changes to MD.

The relationship between the characteristic lengths of mass and thermal diffusion is typically described by the Lewis number ( $L_e$ ), a dimensionless variable defined as

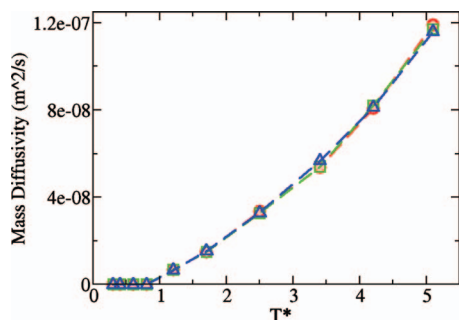


FIG. 6. Mass diffusion coefficient in solid and liquid samples for  $C^{\text{int}} = 0k_B$  (circles),  $10k_B$  (squares), and  $25k_B$  (triangles). The mass diffusion coefficient is zero in all solid samples while it increases with temperature in liquid samples. The effect of internal specific heat is negligible in all cases.

$$L_e^{-1} = \frac{D_{\text{mass}}}{\alpha}. \quad (14)$$

Similarly, we define a local Lewis ( $L_e'$ ) that is related to the local thermal diffusivity as

$$L_e'^{-1} = \frac{D_{\text{mass}}}{\alpha'}. \quad (15)$$

The temperature dependence of  $L_e^{-1}$  and  $L_e'^{-1}$  is shown in Fig. 7. For solid samples, zero  $D_{\text{mass}}$  and nonzero  $\alpha$  leads to zero  $L_e^{-1}$ .  $L_e'^{-1}$  is not shown for these cases since both  $D_{\text{mass}}$  and  $\alpha'$  are too small to measure accurately using molecular simulations. For liquid samples, the inverse of Lewis number  $L_e^{-1}$  increases with both temperature and  $C^{\text{int}}$ , indicating that thermal diffusion is catching up with mass diffusion as temperature and specific heat increase. The inverse of local Lewis number  $L_e'^{-1}$ , on the other hand, is essentially unity ( $1 \pm 0.05$  from our numerical simulations), showing that the energy diffusion coefficient of the internal DoFs corresponds to the mass diffusion coefficient. The enhanced thermal conduction in liquid samples with nonzero  $C^{\text{int}}$  is essentially the result of improved mass diffusion. When temperature is low and the mesoparticles are in the solid state, mass diffusion is negligible and the amount of energy stored in the internal DoFs is not transported; increasing  $C^{\text{int}}$  leads to an increase in this nontransferable energy and therefore does not help thermal conduction. Once the temperature is increased above  $T_m$  and the material turns into a liquid with nonzero mass

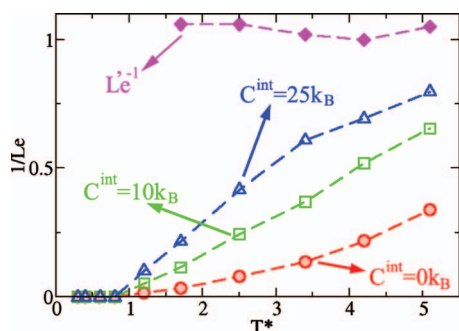


FIG. 7. Inverse of Lewis number with nominal temperature  $T^*$  for  $C^{\text{int}} = 0k_B$  (circles),  $10k_B$  (squares), and  $25k_B$  (triangles) together with  $L_e'^{-1}$  calculated using local thermal diffusivity  $\alpha'$ .  $L_e^{-1}$  increases with temperature and  $C^{\text{int}}$  while  $L_e'^{-1}$  remains constantly at 1 for liquid samples.

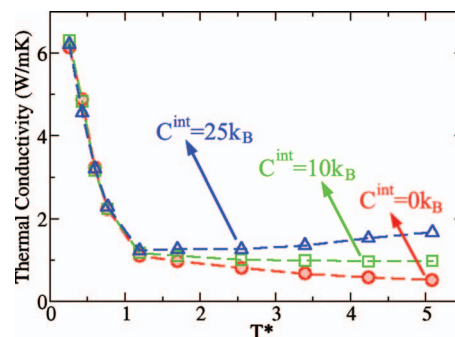


FIG. 8. Thermal conductivity as a function of nominal temperature  $T^*$  for three mesoparticle systems of  $C^{\text{int}} = 0k_B$  (circles),  $10k_B$  (squares), and  $25k_B$  (triangles). The three curves overlap at low temperatures but split when temperature is increased beyond the melting temperature.

diffusion coefficient, the mesoparticles become mobile and so do their internal DoFs and the energy associated with them. The behavior of the internal DoFs is similar to that of the nonpropagating modes in amorphous materials such as silica<sup>31</sup> and amorphous silicon.<sup>32,33</sup>

The relationships between temperature, internal specific heat, and thermal conductivity are further investigated by comparing the temperature dependence of thermal conductivity in systems of different internal specific heats:  $C^{\text{int}} = 0k_B$ ,  $10k_B$ , and  $25k_B$ . The coupling rate used in the simulations is  $2.066 \text{ ps}^{-1}$  in all cases. As shown in Fig. 8, at low temperatures when the systems are in the solid phase, the three curves overlap since the contribution of internal DoFs to thermal conduction is negligible. In this temperature regime, thermal conductivity decreases with increasing temperature in all of the three cases due to enhanced phonon scattering. As the temperature is increased over  $T_m$  and the systems turn into the liquid phase, thermal conductivity of the system of zero  $C^{\text{int}}$  keeps decreasing with temperature—a behavior predicted and observed in a number of liquid molecular crystals.<sup>34–36</sup> The negative slope of thermal conductivity versus temperature curve is reduced when  $C^{\text{int}}$  is increased to  $10k_B$ , as a result of the activated thermal role of internal DoFs at high temperatures (due to enhanced mass diffusion) that partly compensates for the reduced thermal conduction due to increased scattering. This trend agrees with the experimental results by Touloukian and co-workers<sup>37</sup> for thermal conductivity of liquid paraffin hydrocarbons of various molecular weights: thermal conductivity generally decreases with temperature, while larger molecular weight [proportional to  $N^{\text{atom}} = (N^{\text{int}} + 3)/3$  in our case] leads to higher thermal conductivity at the same temperature and decreased temperature dependence. A theoretical work by Bedrov and co-workers<sup>38</sup> using atomistic MD simulations also predicts a very weak temperature dependence of thermal conductivity for liquid HMX, a high-energy density nitramine. For our model system we observe an increase in thermal conductivity with temperature when  $C^{\text{int}}$  is increased to  $25k_B$ , indicating that the role of the internal DoFs is dominating the thermal conduction of the mesoparticle system. This seems to be the case in the MD simulations in Ref. 38 for HMX (with 28 atoms per molecule) at the highest temperatures explored.

## V. QUANTUM CORRECTIONS TO ALL-ATOM MD SIMULATIONS

The main result of Sec. IV, i.e., the fact that the local thermal diffusivity is equal to the mass diffusivity ( $\alpha' = D_{\text{mass}}$ ), enables a practical approach to incorporate quantum corrections to all-atom MD simulations of thermal transport in molecular fluids based on quantities that can be computed accurately and easily.

As mentioned in Sec. I, being based on classical mechanics, MD leads to results consistent with classical, not quantum, statistical mechanics. This leads to an incorrect description of high frequency rotovibrational DoFs with energy  $h\nu$  higher than or comparable to  $kT$ . Classically all DoFs can have any possible energy, including values smaller than the energy quantum  $h\nu$ , leading to an overestimation of specific heat at low temperatures. As we saw in the previous section this overestimate will lead to an inaccurate description of thermal conductivity of liquid samples. Thermal conductivity obtained from MD simulations can be written as having the contributions from the molecular and internal DoFs

$$\kappa_{\text{MD}} = \kappa^{\text{mol}} + \frac{D_{\text{mass}}}{V} C^{\text{int}}, \quad (16)$$

where the first and second terms on the right hand side of the equation represent the intermolecular and intramolecular shares of thermal conductivity, respectively, and  $V$  is the atomic volume. Among these quantities,  $\kappa^{\text{mol}}$  is associated with low frequency intermolecular interactions and therefore is accurately described by MD. Mass diffusion also involves low frequency, low energy DoFs and a classical MD simulation will lead to an accurate mass diffusivity if an appropriate interatomic potential is used. The internal specific heat, on the other hand, is the only quantity that is described inaccurately in MD and needs correction. As we showed in Sec. IV, the contribution of the internal DoFs to thermal conduction in MD simulations is  $C_{\text{CM}}^{\text{int}} D_{\text{mass}}$  (where the CM subscript denotes classical mechanics) but their contribution should be  $C_{\text{QM}}^{\text{int}} D_{\text{mass}}$  with a quantum mechanical specific heat. Therefore, a quantum corrected thermal conductivity  $\kappa_{\text{QM}}$  can be computed based on the one obtained from MD as

$$\kappa_{\text{QM}} = \kappa_{\text{MD}} + \frac{D_{\text{mass}}}{V} (-C_{\text{CM}}^{\text{int}} + C_{\text{QM}}^{\text{int}}). \quad (17)$$

$C_{\text{CM}}^{\text{int}}$  and  $C_{\text{QM}}^{\text{int}}$  are the classical and quantum mechanical heat capacity and their difference can be estimated very accurately from the quasiharmonic vibrational density of states computed from the velocity power spectrum.<sup>22</sup>

## VI. CONCLUSIONS

We used the thermodynamically accurate mesoscale method DID to investigate the role of internal DoFs on thermal conduction in a model molecular crystal. Thermal conductivity is calculated based on Fourier's law via results from nonequilibrium mesodynamics simulations.

We characterize the effects of internal specific heat on thermal conductivity in a model molecular material. While localized, internal DoFs play a negligible role in thermal transport in solid samples, for liquid samples we find a linear

relationship between  $C^{\text{int}}$  and thermal conductivity. The slope of the thermal conductivity versus  $C^{\text{int}}$  curve increases with temperature, showing an increasingly stronger role of internal DoFs as the mobility of the mesoparticles is enhanced. The coefficient of proportionality, i.e., the local thermal diffusivity, is found to be of the same value to the mass diffusivity under all the conditions we could test numerically for all our liquid samples.

The contribution of internal DoFs to thermal conduction can be very important at elevated temperatures. As temperature increases, the contribution of internal DoFs can compensate for the reduction in thermal conductivity by molecular DoFs due to increased scattering, and even improve the overall thermal conductivity of the molecular fluid.

Finally, it should be noted that, given the data and expression of the electron specific heat and coupling rate, the DID approach can be modified to describe the coupled thermal transport of phonons and electrons in metallic systems, where the mesoparticles are replaced by ions and the internal DoFs replaced by the electronic DoFs.

## ACKNOWLEDGMENTS

This work was partially supported by Purdue University and the Network for Computational Nanotechnology through nanoHUB.org computational resources funded by the U.S. National Science Foundation Grant No. EEC-0228390.

- <sup>1</sup>J. A. Eastman, S. U. S. Choi, S. Li, W. Yu, and L. J. Thompson, *Appl. Phys. Lett.* **78**, 718 (2001).
- <sup>2</sup>B. Yang and Z. H. Han, *Appl. Phys. Lett.* **89**, 083111 (2006).
- <sup>3</sup>X. Yu and D. M. Leitner, *J. Chem. Phys.* **119**, 12673 (2003).
- <sup>4</sup>N. Shenogina, P. Keblinski, and S. Garde, *J. Chem. Phys.* **129**, 155105 (2008).
- <sup>5</sup>S. Melchionna, G. Briganti, P. Londei, and P. Cammarano, *Phys. Rev. Lett.* **92**, 158101 (2004).
- <sup>6</sup>T. Matsuda, M. Kikuchi, Y. Tanaka, M. Hiraoka, Y. Nishimura, K. Akuta, M. Takahashi, M. Abe, N. Fuwa, and K. Morita, *Int. J. Hyperthermia* **7**, 425 (1991).
- <sup>7</sup>J. Liu, *Prog. Nat. Sci.* **10**, 787 (2000).
- <sup>8</sup>Z. Wang, J. A. Carter, A. Lagutchev, Y. K. Koh, N. H. Seong, D. G. Cahill, and D. D. Dlott, *Science* **317**, 787 (2007).
- <sup>9</sup>T. H. Tsai, L. S. Kuo, P. H. Chen, and C. T. Yang, *Appl. Phys. Lett.* **93**, 233121 (2008).
- <sup>10</sup>D. G. Cahill, K. Goodson, and A. Majumdar, *ASME J. Heat Transfer* **124**, 223 (2002).
- <sup>11</sup>K. Kremer, *Macromol. Chem. Phys.* **204**, 257 (2003).
- <sup>12</sup>F. Müller-Plathe, *ChemPhysChem* **3**, 754 (2002).
- <sup>13</sup>M. Pickholz, L. Saiz, and M. L. Klein, *Biophys. J.* **88**, 1524 (2005).
- <sup>14</sup>P. Derreumaux and N. Mousseau, *J. Chem. Phys.* **126**, 025101 (2007).
- <sup>15</sup>A. Strachan and B. L. Holian, *Phys. Rev. Lett.* **94**, 014301 (2005).
- <sup>16</sup>H. S. Ashbaugh, H. A. Patel, S. K. Kumar, and S. Garde, *J. Chem. Phys.* **122**, 104908 (2005).
- <sup>17</sup>Y. Mishin, M. J. Mehl, and D. A. Papaconstantopoulos, *Phys. Rev. B* **65**, 224114 (2002).
- <sup>18</sup>Y. Zhou, B. Anglin, and A. Strachan, *J. Chem. Phys.* **127**, 184702 (2007).
- <sup>19</sup>V. Molinero and W. A. Goddard III, *J. Phys. Chem. B* **108**, 1414 (2004).
- <sup>20</sup>B. L. Holian, *Europhys. Lett.* **64**, 330 (2003).
- <sup>21</sup>K. Lynch, A. Thompson, and A. Strachan, *Modell. Simul. Mater. Sci. Eng.* **17**, 015007 (2009).
- <sup>22</sup>P. H. Berens, D. H. J. Mackay, G. M. White, and K. R. Wilson, *J. Chem. Phys.* **79**, 2375 (1983).
- <sup>23</sup>H. J. C. Berendsen, J. P. M. Postma, W. F. v. Gunsteren, A. DiNola, and J. R. Haak, *J. Chem. Phys.* **81**, 3684 (1984).
- <sup>24</sup>F. Müller-Plathe, *J. Chem. Phys.* **106**, 6082 (1997).
- <sup>25</sup>I. Ponomareva, D. Srivastava, and M. Menon, *Nano Lett.* **7**, 1155 (2007).

- <sup>26</sup>R. W. Klaffky, N. S. Mohan, and D. H. Damon, *Phys. Rev. B* **11**, 1297 (1975).
- <sup>27</sup>S. N. Luo, A. Strachan, and D. C. Swift, *J. Chem. Phys.* **120**, 11640 (2004).
- <sup>28</sup>*Thermal Conductivity: Theory, Properties, and Applications*, edited by T. Tritt (Kluwer Academic/Plenum, New York, 2004).
- <sup>29</sup>P. B. Allen, *Phys. Rev. B* **48**, 12581 (1993).
- <sup>30</sup>S. Sarkar and R. P. Selvam, *J. Appl. Phys.* **102**, 074302 (2007).
- <sup>31</sup>X. Yu and D. M. Leitner, *Phys. Rev. B* **74**, 184305 (2006).
- <sup>32</sup>B. L. Zink, R. Pietri, and F. Hellman, *Phys. Rev. Lett.* **96**, 055902 (2006).
- <sup>33</sup>D. Donadio and G. Galli, *Phys. Rev. Lett.* **102**, 195901 (2009).
- <sup>34</sup>P. J. Davis and D. J. Evans, *Chem. Phys.* **198**, 25 (1995).
- <sup>35</sup>R. J. Hulse, M. W. Anderson, M. D. Bybee, D. D. Gonda, C. A. Miller, J. L. Oscarson, R. L. Rowley, and W. V. Wilding, *J. Chem. Eng. Data* **49**, 1433 (2004).
- <sup>36</sup>F. Civan, *Chem. Eng. Sci.* **63**, 5883 (2008).
- <sup>37</sup>Y. S. Touloukian, P. E. Liley, and S. C. Saxena, *Thermophysical Properties of Matter* (IFI/Plenum, New York, 1970).
- <sup>38</sup>D. Bedrov, G. D. Smith, and T. D. Sewell, *Chem. Phys. Lett.* **324**, 64 (2000).